Scientific paper

Synthesis, Crystal Structure, Photophysical Properties and Theoretical Study of a New Iridium(III) Complex Containing 2-phenylbenzothiazole Ligand

Yong-Pi Zeng,[1] Cheng-Wei Gao,[1] Liang-Jiang Hu,[1] Hao-Hua Chen,[1] Guang-Ying Chen,[2] Gao-Nan Li[1,*] and Zhi-Gang Niu[1,2,*]

[1] *College of Chemistry and Chemical Engineering, Hainan Normal University, Haikou 571158, China*

[2] *Key Laboratory of Tropical Medicinal Plant Chemistry of Ministry of Education, Hainan Normal University, Haikou 571158, China*

** Corresponding author: E-mail: ligaonan2008@163.com, niuzhigang1982@126.com*

Received: 08-06-2015

Abstract

A new bis-cyclometalated iridium(III) complex [Ir(dmabt)$_2$(bipy)][PF_6] (**3**) (dmabt = 4-(benzo[*d*]thiazol-2-yl)-*N*,*N*-dimethylaniline, bipy = 2,2'-bipyridine) has been synthesized and fully characterized. The structure of complex **3** has been determined by X-ray analyses which shows that the central iridium(III) ion assumes distorted octahedral geometry. The photoluminescence spectrum exhibits orange emission maximum at 612 nm with quantum yield of 17% at 298 K. The frontier molecular orbital diagrams and the spin-allowed singlet-singlet electronic transitions of **3** have been calculated with density functional theory (DFT) and time-dependent DFT (TD-DFT), and the UV-Vis spectra are discussed based on the theoretical calculations.

Keywords: Iridium(III) complex; 2-phenylbenzothiazole; Syntheses; Crystal structure; Photoluminescence; DFT calculation

1. Introduction

In recent decades, organic light-emitting diodes (OLEDs) have received considerable attention as a promising technology for practical optoelectronic applications.[1–3] Particularly, luminescent iridium-based complexes play an important role in the fabrication of efficient OLEDs on account of their high stability, large quantum efficiency, short excited-stated lifetime and excellent color tunability.[4,5] Moreover, substantial researches on iridium complexes have showed that the emission wavelength can be tuned by judicious selection of various ligands, which can be further refined by altering the ligand substituents.[6] In 2004, the research group lead by T. M. Chen et al. has synthesized and reported a series of iridium(III) complexes with 2-phenylbenzothiazole-based ligands. And they confirmed that varying the substituents (–CF_3, –F, –Me, –OMe) on the 2-phenylbenzothiazole ligands could fine-tune their solution-state photophysical properties.[7] In this paper, we report on the introduction of a stronger electron-donating group [–N(Me)$_2$] as the substituent. Based on the new 2-phenylbenzothiazole-based ligand (**1**), the corresponding Ir(III) complex **3** has been synthesized. The photophysical properties of **3** are investigated and the absorption spectra are rationalized on the basis of density functional theory (DFT) and time-dependent DFT (TDDFT).

2. Experimental

2. 1. Materials and Instrumentations

4-(Dimethylamino)benzaldehyde and 2-aminobenzenethiol were obtained from Sigma Adrich. $IrCl_3 \cdot 3H_2O$ was industrial product. All commercial chemicals were used without further purification unless otherwise stated. Solvents were dried and degassed following standard procedures. ^{1}H NMR and ^{13}C NMR spectra were recorded on a Bruker AM 400 MHz instrument. Chemical shifts were reported in ppm relative to Me_4Si

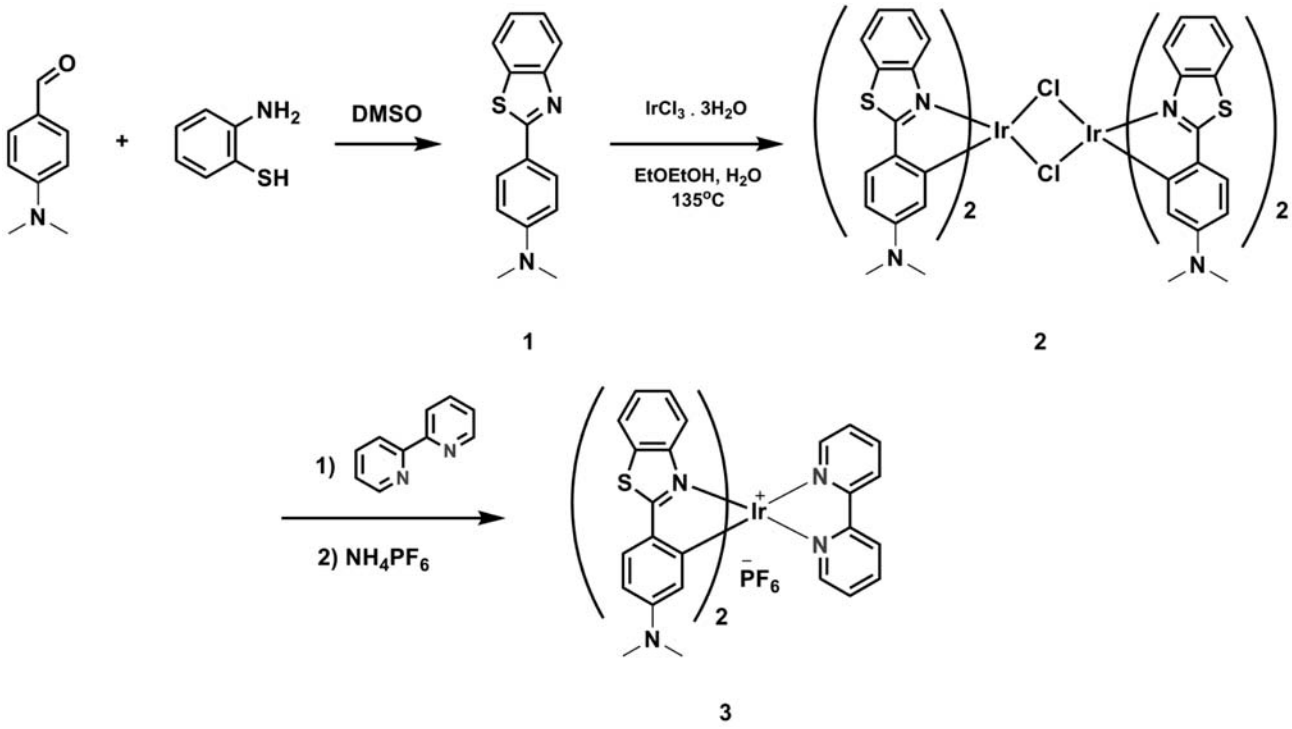

Scheme 1. Synthetic routes of Ir(III) complex **3**.

as internal standard. ESI-MS spectra were recorded on an Esquire HCT-Agilent 1200 LC/MS spectrometer. FT-IR spectra were taken on a Nicolet 6700 FTIR spectrometer (400–4000 cm^{-1}) with KBr pellets. Elemental analyses for C, H, and N were performed on a Vario EL Elemental Analyser. UV-Vis spectra were recorded on a Hitachi U3900/3900H spectrophotometer. Fluorescence spectra were carried out on a Hitachi F-7000 spectrophotometer.

2. 2. Synthesis of 4-(benzo[d]thiazol-2-yl)-N,N-dimethylaniline (dmabt, 1)

A mixture of 4-(dimethylamino)benzaldehyde (500 mg, 3.35 mmol) and 2-aminobenzenethiol (420 mg, 3.35 mmol) in DMSO (20 mL) was stirred at 100 °C for 10 h. After cooling, the solution was poured into ice water and extracted with DCM. The combined organic layer was washed with brine, dried over Na_2SO_4 and evaporated. The residue was purified by column chromatography (PE : EA = 20 : 1, R_f = 0.35) to afford pure product **1** (798 mg, yield: 93.6%) as a white solid. IR (KBr, cm^{-1}): 2902 (w), 2809(w), 1610(vs), 1484(vs), 1430(s), 1186 (s), 1065 (m), 963(m), 817(s), 751(s); ^{1}H NMR (400 MHz, $CDCl_3$) 7.95č7.99 (m, 3H), 7.84 (d, *J* = 7.6 Hz, 1H), 7.43 (t, *J* = 7.6 Hz, 1H), 7.30 (t, *J* = 7.6 Hz, 1H), 6.75 (d, *J* = 8.0 Hz, 2H), 3.06 (s, 6H); ^{13}C NMR (100 MHz, $CDCl_3$) 168.9, 154.6, 152.3, 134.7, 129.0, 126.1, 124.3, 122.4, 121.6, 121.5, 111.8, 40.3; MS-ESI: m/z 255.2 (M+1); Anal. Calcd for $C_{15}H_{14}N_2S$: C, 70.83; H, 5.55; N, 11.01; Found: C, 70.72; H, 5.50; N, 11.13.

2. 3. Synthesis of $[Ir(dmabt)_2(bipy)][PF_6]$ (3)

A mixture of $IrCl_3 \cdot 3H_2O$ (63 mg, 0.18 mmol) and the ligand **1** (100 mg, 0.39 mmol) in 9 mL of ethoxyethanol and H_2O (v : v = 2 : 1) was refluxed for 12 h. Upon cooling to room temperature, the orange precipitate was collected by filtration and washed with cooled ether and MeOH. After drying, the crude product of chlorido-bridged dimer complex **2** was used directly in next step without further purification. A mixture of the above dimer complex **2** (80 mg) and 2,2'-bipyridine (21 mg, 2.5 equiv.) was dissolved in 6 mL of DCM and MeOH (v : v = 1 : 1) and was refluxed for 6 h under nitrogen. The orange-red solution was then cooled to room temperature, and NH_4PF_6 (5.0 equiv.) was added to the solution. The mixture was stirred at room temperature for 4 h, and then evaporated to dryness. The solid was purified by column chromatography with DCM / MeOH (100 : 1, R_f = 0.3) eluent to afford pure product **3** (54 mg, yield: 49.6%) as a yellow solid. IR (KBr, cm^{-1}): 2963 (s), 2925(w), 2854(w), 1578(s), 1426(s), 1391(s), 1261 (vs), 1020 (vs), 799(vs), 755(s); UV–Vis (nm): 242, 268, 295, 335, 392, 418, 436; ^{1}H NMR (400 MHz, $CDCl_3$) 8.55 (d, *J* = 8.0 Hz, 2H), 8.13č8.18 (m, 4H), 7.69 (d, *J* = 7.6 Hz, 2H), 7.59 (d, *J* = 8.8 Hz, 2H), 7.17 (t, *J* = 7.6 Hz, 2H), 6.98 (t,

J = 7.6 Hz, 2H), 6.38 (dd, J_1 = 2.4 Hz, J_2 = 8.8 Hz, 2H), 6.02 (d, J = 8.4 Hz, 2H), 5.61 (d, J = 2.0 Hz, 2H), 2.63 (s, 12H). ^{13}C NMR (100 MHz, $CDCl_3$) 179.0, 155.7, 151.9, 151.3, 150.0, 148.7, 138.8, 136.1, 129.4, 127.1, 126.9, 126.7, 123.7, 123.5, 122.0, 115.7, 113.6, 106.2, 38.6; MS-ESI: m/z 855.2 $[MPF_6^-]^+$. Anal. Calcd for $C_{40}H_{34}F_6IrN_6PS_2$: C, 48.04; H, 3.43; N, 8.40; Found: C, 48.11; H, 3.29; N, 8.53.

2. 4. Crystallographic Studies

X-ray diffraction data were collected with an Agilent Technologies Gemini A Ultra diffractometer equipped with graphite-monochromated Mo Kα radiation (λ = 0.71073 Å) at room temperature. Data collection and reduction were processed with CrysAlisPro software.[8] The structure was solved and refined using full-matrix least-squares based on F^2 with program SHELXS-97 and SHELXL-97[9] within Olex2.[10] All non-hydrogen atoms were found in alternating difference Fourier syntheses and least-squares refinement cycles and, during the final cycles, refined anisotropically. Hydrogen atoms were placed in calculated positions and refined as riding atoms with a uniform value of U_{iso}.

2. 5. Computational Method

The geometry of complex **3** was optimized starting from the X-ray data by the DFT (density functional theory) method with B3LYP (Becke three-parameter Lee-Yang-Parr) hybrid density functional theory and the 6-31G* basis set. All calculations were carried out with Gaussian 09 software package.[11]

2. 6. Luminescence Quantum Efficiency

The luminescence quantum efficiencies were calculated by comparison of the fluorescence intensities (integrated areas) of a standard sample *fac*-Ir(ppy)$_3$ and the unknown sample according to the equation.[12–14]

$$\Phi_{unk} = \Phi_{std}\left(\frac{I_{unk}}{I_{std}}\right)\left(\frac{A_{std}}{A_{unk}}\right)\left(\frac{\eta_{unk}}{\eta_{std}}\right)^2$$

Where Φ_{unk} and Φ_{std} are the luminescence quantum yield values of the unknown sample and *fac*-Ir(ppy)$_3$ solutions (Φ_{std} = 0.4),[14] respectively. I_{unk} and I_{std} are the integrated fluorescence intensities of the unknown sample and *fac*-Ir(ppy)$_3$ solutions, respectively. A_{unk} and A_{std} are the absorbance values of the unknown sample and *fac*-Ir(ppy)$_3$ solutions at their excitation wavelengths, respectively. The η_{unk} and η_{std} terms represent the refractive indices of the corresponding solvents (pure solvents were assumed).

3. Results and Discussion

3. 1. Description of Crystal Structure

The crystal of **3** suitable for X-ray structural analysis was obtained by slow evaporation of CH_2Cl_2/MeOH solution. The crystallographic data and structure refinement details are given in Table S1; selected bond lengths and bond angles are collected in Table S2.

ORTEP view of complex **3** with the atomic numbering scheme is shown in Fig. 1. It crystallizes in triclinic space group P $\bar{1}$ and the asymmetric unit comprises two molecules. As seen, the Ir(III) ion resides in a distorted octahedral $[(C\hat{}N)_2Ir(N\hat{}N)]^+$ coordination geometry with the C and N atoms of two dmabt (C^N) ligands and the two N atoms of bipy (N^N) ligand. Moreover, two cyclometalated dmabt ligands adopt *cis*-C,C and *trans*-N,N configuration.[15] Among all the coordination bonds, the Ir-N_{bipy} bonds are the longest (2.114–2.133 Å). It is not surprising to find that the Ir–C bonds (1.996–2.022 Å) are shorter than Ir–N_{dmabt} bonds (2.044–2.056 Å), suggesting the stronger coordination effect of Ir–C bonds than Ir–N bonds.[16] After coordinated to Ir(III) ion, the phenyl ring (C18–C19–C20–C21–C22–C23) is almost fixed in the parallel position with the benzothiazole ring, and the dihedral angle between the two rings is 11.577°.

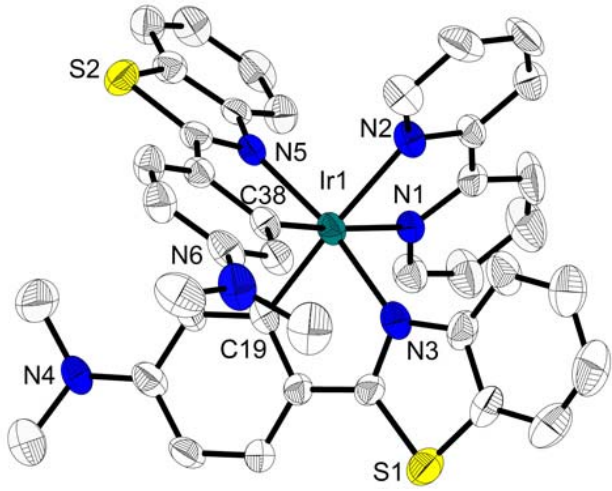

Fig. 1. ORTEP view of **3** with the thermal ellipsoids drawn at the 30% probability level. Hydrogen atoms, solvent molecules and PF_6 anion are omitted for clarity. Selected bond length and angles: Ir(1)-N(1), 2.114(9); Ir(1)-N(2), 2.133(8); Ir(1)-N(3), 2.056(8); Ir(1)-N(5), 2.044(7); Ir(1)-C(19), 2.022(8); Ir(1)-C(38), 1.996(10); N(3)-Ir(1)-N(5), 170.2(3); C(19)-Ir(1)-N(2), 174.6(4); C(38)-Ir(1)-N(1), 173.7(3); N(5)-Ir(1)-N(2), 91.1(3); N(5)-Ir(1)-N(1), 101.4(3); N(5)-Ir(1)-C(19), 91.0(3); N(5)-Ir(1)-C(38), 80.1(3); C(19)-Ir(1)-C(38), 88.0(3); N(1)-Ir(1)-N(2), 76.5(3); N(3)-Ir(1)-N(2), 97.9(3).

3. 2. Electronic Absorption Spectra

The UV-Vis absorption spectra of **3** in CH_2Cl_2 solution are presented along with the calculated spectra (Fig. 2). The absorption band at 243 nm is assigned to the spin-

allowed ligand-centered $^1\pi$–π^* transitions arising from N^N ligands. The next absorption bands up to ca. 320 nm are assigned to the spin-allowed ^{1}MLCT transitions from the Ir(III) center to the C^N ligands. The strongest band at 436 nm is assigned to LLCT transitions from C^N ligands to N^N ligands.

The electronic absorption spectra of **3** were calculated using the time-dependent density functional theory (TD-DFT) method. The calculated results and spin-allowed electronic transitions are listed in Table 1, as well as compared with the experimental absorption spectra data. The molecular HOMO/LUMO orbital pictures are presented in Fig. 3. The electron density distributions are summarized in Table S3.

As can be seen from Fig. 2, agreement between the calculated UV-Vis spectra and the experimentally determined spectra is quite satisfactory. According to the Fig. 2 and Table 1, electronic absorption spectra of **3** mainly exhibits four bands at 436, 295, 268 and 242 nm arising from corresponding electronic transition between HOMO/HOMO–1 and LUMO+1/LUMO+2/LUMO+3, HOMO–2 and LUMO+2, HOMO–5 and LUMO+1 orbitals, respectively. Unlike other iridium complexes,[17,18] the highest molecular orbital (HOMO) is mainly localized on the dmabt ligand, whereas the lowest unoccupied molecular orbital (LUMO) is mainly delocalized on the bipyridine ligand. As a result, the lowest-energy electronic transition (436 nm) is not derived from HOMO → LUMO transition, which corresponds to ligand-ligand charge-transfer (LLCT, $L_{dmabt}(\pi) \rightarrow L_{bipy}(\pi^*)$, Table 1).

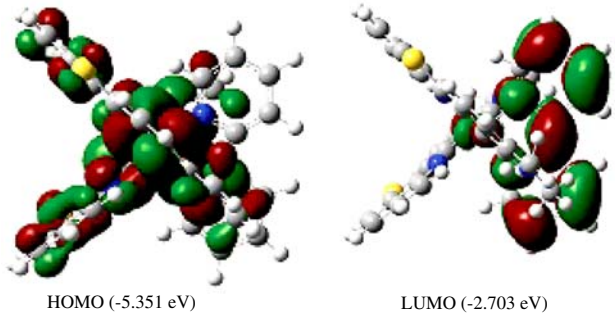

Fig. 3. The frontier molecular orbital diagrams of complex **3** from DFT calculations.

3. 3. Emission Properties

Photoluminescence measurement was conducted in degassed CH_2Cl_2 solution at room temperature (Fig. 4). Upon photoexcitation at ca. 437 nm, complex **3** shows orange luminescence with the emission peak appeared at 612

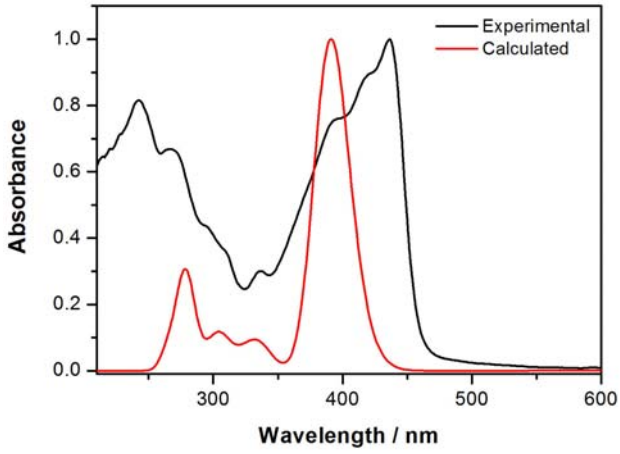

Fig. 2. Comparison between the experimental and calculated UV–Vis absorption spectra of **3**.

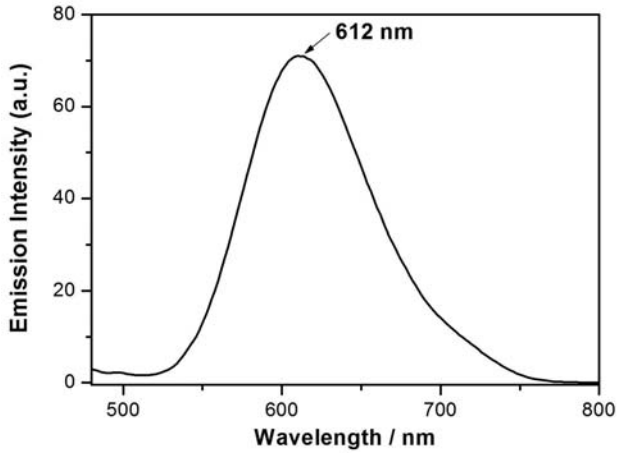

Fig. 4. The emission spectra of **3** in CH_2Cl_2 at room temperature.

Table 1 Main experimental and calculated optical transitions for **3**.

Orbital Excitations	Character	Oscillation Strength	Calcd (nm)	Exptl (nm)
HOMO → LUMO+2 HOMO → LUMO+3	$L_{dmabt}(\pi) \rightarrow L_{dmabt/Bipy}(\pi^*)$	0.2985	390	436
HOMO → LUMO+1 HOMO–1 → LUMO+3	$L_{dmabt}(\pi) \rightarrow L_{dmabt/Bipy}(\pi^*)$	0.9249	389	
HOMO–2 → LUMO+2	$Ir(d\pi)/L_{dmabt}(\pi) \rightarrow L_{dmabt}(\pi^*)$	0.0912	335	295
HOMO–5 → LUMO+1	$Ir(d\pi)/L_{dmabt}(\pi) \rightarrow L_{dmabt}(\pi^*)$	0.0738	304	268
HOMO–12 → LUMO	$L_{Bipy}(\pi) \rightarrow L_{Bipy}(\pi^*)$	0.3239	279	242

nm. From the results of UV-Vis spectra and DFT calculations, it can be seen that the emissive excited state arise from intraligand π–π^* relaxation. In addition, phosphorescence relative quantum yield (Φ) in dichloromethane solution was measured to be 0.17 at room temperature by using typical phosphorescent *fac*-Ir(ppy)$_3$ as a standard (Φ = 0.40).[14]

4. Conclusions

In summary, a new bis-cyclometalated 2-phenylbenzothiazole-based iridium(III) complex **3** has been successfully prepared and characterized. Structural studies indicated that complex **3** adopts a distorted octahedral geometry around the iridium metal exhibiting *cis*-C,C' and *trans*-N,N' chelate disposition. The absorption and emission spectra have been investigated. The spin-allowed singlet-singlet electronic transitions are calculated with time-dependent DFT (TD–DFT), and a good agreement with the experimental data is observed.

5. Acknowledgements

This work was supported by the Natural Science Foundation of Hainan Province (No. 20152017), the Science and Research Project of Education Department of Hainan Province (Nos. Hjkj2013-25 and Hnky2015-27), Hainan Provincial Innovation Experiment Program for University Students (No. 20140053) and Hainan Normal University's Innovation Experiment Program for University Students (No. cxcyxj2015005).

6. Supplementary Material

Crystallographic data for the structural analyses have been deposited in the Cambridge Crystallographic Data Centre, CCDC reference number 1404920. Copies of this information may be obtained free of charge from The Director, CCDC, 12 Union Road, Cambridge CB2 1EZ, UK (fax: +44 1223 336033; e-mail: deposit@ccdc.cam. ac.uk or).

7. References

1. M. A. Baldo, M. E. Thompson, S. R. Förrest, *Pure. Appl. Chem*. **1999**, *71*, 2095–2106. http://dx.doi.org/10.1351/pac199971112095
2. M. Ikai, S. Tokito, Y. Sakamoto, T. Suzuki, Y. Taga, *Appl. Phys. Lett*. **2001**, *79*, 156–158. http://dx.doi.org/10.1063/1.1385182
3. S.-C. Lo, N. A. H. Male, J. P. J. Markham, S. W. Magennis, P. L. Burn, O. V. Salata, I. D. W. Samuel, *Adv. Mater*. **2002**, *14*, 975–979. http://dx.doi.org/10.1002/1521-4095(20020705)14:13/14<975::AID-ADMA975>3.0.CO;2-D
4. M. A. Baldo, C. Adachi, S. R. Forrest, *Phys. Rev. B* **2000**, *62*, 10967–10977. http://dx.doi.org/10.1103/PhysRevB.62.10967
5. J. M. Lupton, I. D. W. Samuel, M. J. Frampton, R. Beavington, P. L. Burn, Adv. Funct. Mater. **2001**, *11*, 287–294. http://dx.doi.org/10.1002/1616-3028(200108)11:4<287::AID-ADFM287>3.0.CO;2-Z
6. F. Neve, M. La Deda, A. Crispini, A. Bellusci, F. Puntoriero, S. Campagna, *Organometallics* **2004**, *23*, 5856–5863. http://dx.doi.org/10.1021/om049493x
7. I. R. Laskar, T. M. Chen, *Chem. Mater.* **2004**, *16,* 111–117. http://dx.doi.org/10.1021/cm030410x
8. CrysAlisPro Version 1.171.36.21. Agilent Technologies Inc. Santa Clara, CA, USA, **2012**.
9. G. M. Sheldrick, *Acta. Cryst.* **2008**, *A64*, 112–122. http://dx.doi.org/10.1107/S0108767307043930
10. O. V. Dolomanov, L. J. Bourhis, R. J. Gildea, J. A. K. Howard, H. Puschmann, *J. Appl. Cryst.* **2009**, *42*, 339–341. http://dx.doi.org/10.1107/S0021889808042726
11. M. J. Frisch, G. W. Trucks, H. B. Schlegel, et al, Gaussian 09, Revision A.01; Gaussian, Inc.: Wallingford, CT, **2009**.
12. A. Juris, V. Balzani, F. Barigelletti, S. Campagna, P. Belser, A. von Zelewsky *Coord. Chem. Rev.* **1988**, *84*, 85–277. http://dx.doi.org/10.1016/0010-8545(88)80032-8
13. M. Frank, M, Nieger, F, Vögtle, P. Belser, A. Vonzelewsky, L. D. Cola, V. Balzani, F. Barigelletti, L. Flamigni, *Inorg. Chim. Acta.* **1996**, *242*, 281–291. http://dx.doi.org/10.1016/0020-1693(95)04878-2
14. K. A. King, P. J. Spellane, R. J. Watts, *J. Am. Chem. Soc.* **1985**, *107*, 1431–1432. http://dx.doi.org/10.1021/ja00291a064
15. G. N. Li, Y. Zou, Y. D. Yang, J. Liang, F. Cui, T. Zheng, H. Xie, Z. G. Niu, *J. Fluoresc.*, **2014**, *24*, 1545–1552. http://dx.doi.org/10.1007/s10895-014-1443-7
16. T. Y. Li, X. Liang, C. Wu, L. S. Xue, Q. L. Xu, S. Zhang, X. Liu, Y. X. Zheng, X. Q. Wang, *J. Organometal. Chem.* **2014**, *755*, 110–119.
17. Z. G. Niu, D. Liu, J. Zuo, Y. Zou, J. M. Yang, Y. H. Su, Y. D. Yang, G. N. Li, *Inorg. Chem. Commun*. **2014**, *43*, 146–150. http://dx.doi.org/10.1016/j.inoche.2014.02.031
18. Q. Zhao, F. Y. Li, S. J. Liu, M. X Yu, Z. Q Liu, T. Yi, C. H. Huang, *Inorg. Chem.* **2008**, *47*, 9256–9264. http://dx.doi.org/10.1021/ic800500c

Povzetek

Sintetiziran in okarakteriziran je nov bis-ciklometaliran iridijev(III) kompleks [Ir(dmabt)$_2$(bipy)][PF$_6$] (**3**) (dmabt = 4-(benzo[*d*]tiazol-2-il)-*N*,*N*-dimetilanilin, bipy = 2,2'-bipiridin). Struktura kompleksa **3** je bila določena z rentgensko analizo, ki je razkrila, da ima centralni iridijev(III) ion popačeno oktaedrično geometrijo. Fotoluminiscenčni spekter vsebuje oranžni emisijski maksimum pri 612 nm s kvantnim izkoristkom 17% pri 298 K. Izračunani so diagrami mejnih molekulskih orbital ter spinsko dovoljeni singlet-singlet elektronski prehodi za spojino **3** po teoriji gostotnostnega funkcionala (DFT) in časovno odvisni DFT (TD-DFT). Rezultati teoretičnih izračunov so bili uporabljeni pri interpretaciji UV-Vis spektrov.

Synthesis, crystal structure, photophysical properties and theoretical study of a new iridium(III) complex containing 2-phenylbenzothiazole ligand

Yong-Pi Zeng,[1] Cheng-Wei Gao,[1] Liang-Jiang Hu,[1] Hao-Hua Chen,[1] Guang-Ying Chen,[2] Gao-Nan Li[1,*] and Zhi-Gang Niu[1,2,*]

[1] *College of Chemistry and Chemical Engineering, Hainan Normal University, Haikou 571158, China*

[2] *Key Laboratory of Tropical Medicinal Plant Chemistry of Ministry of Education, Hainan Normal University, Haikou 571158, China*

* *Corresponding author: E-mail: ligaonan2008@163.com, niuzhigang1982@126.com*

Supporting materials

Table S1 Crystallographic data and structure refinement details for **3**.

Empirical formula	$C_{40}H_{34}F_6IrN_6PS_2$
M_r	1000.02
Crystal system	Triclinic
Space group	$P\bar{1}$
Wavelength / Å	0.71073
X-radiation (graphite monochromator)	Mo-Kα
T / K	293(2)
a (Å)	10.5274(3)
b (Å)	15.7581(6)
c (Å)	23.8577(7)
α (°)	88.861(3)
β (°)	85.958(3)
γ (°)	82.435(3)
V (Å^3)	3913.4(2)
Z	4
D_{calcd} (Mg/m^3)	1.697
F(000)	1976
μ(Mo-Kα)/ mm^{-1}	3.627
index ranges	$-13 \le h \le 13$
	$-19 \le k \le 19$
	$-27 \le l \le 29$
R_{int}	0.0881
GOF (F^2)	0.890
$R_1{}^a$, $wR_2{}^b$ ($I > 2\sigma(I)$)	0.0616, 0.0781
$R_1{}^a$, $wR_2{}^b$ (all data)	0.1507, 0.1041

^{a} $R_1 = \Sigma||F_o| - |F_c||/\Sigma|F_o|$. ^{b} $wR_2 = [\Sigma w(F_o^2 - F_c^2)^2/\Sigma w(F_o^2)]^{1/2}$

Table S2 Selected bond distances (Å) and angles (◦) for complex **3**.

Ir(1)-N(1)	2.114(9)	C(5)-C(6)	1.477(14)
Ir(1)-N(2)	2.133(8)	C(17)-C(18)	1.413(11)
Ir(1)-N(3)	2.056(8)	N(4)-C(21)	1.341(11)
Ir(1)-N(5)	2.044(7)	N(4)-C(24)	1.451(12)
Ir(1)-C(19)	2.022(8)	S(1)-C(16)	1.720(11)
Ir(1)-C(38)	1.996(10)	S(1)-C(17)	1.715(8)
N(3)-Ir(1)-N(5)	170.2(3)	N(5)-Ir(1)-C(19)	91.0(3)
C(19)-Ir(1)-N(2)	174.6(4)	N(5)-Ir(1)-C(38)	80.1(3)
C(38)-Ir(1)-N(1)	173.7(3)	C(19)-Ir(1)-C(38)	88.0(3)
N(5)-Ir(1)-N(2)	91.1(3)	N(1)-Ir(1)-N(2)	76.5(3)
N(5)-Ir(1)-N(1)	101.4(3)	N(3)-Ir(1)-N(2)	97.9(3)

Table S3 Frontier orbital energy and electron density distribution for **3**.

Orbital	Energy (eV)	Composition (%)			
		Ir	Ph-R	benzothiazole	2,2'-bipyridine
LUMO+3	-1.724	5.11	6.43	13.04	75.46
LUMO+2	-1.835	3.12	28.04	50.40	19.23
LUMO+1	-1.842	2.77	34.59	59.50	4.24
LUMO	-2.703	4.70	4.31	0.27	90.78
HOMO	-5.351	0.21	91.62	21.72	1.06
HOMO-1	-5.371	4.25	87.40	22.17	1.06
HOMO-2	-6.247	45.69	51.27	5.12	4.87
HOMO-5	-6.523	31.09	6.12	56.55	8.12
HOMO-12	-7.630	17.85	11.50	3.39	69.78

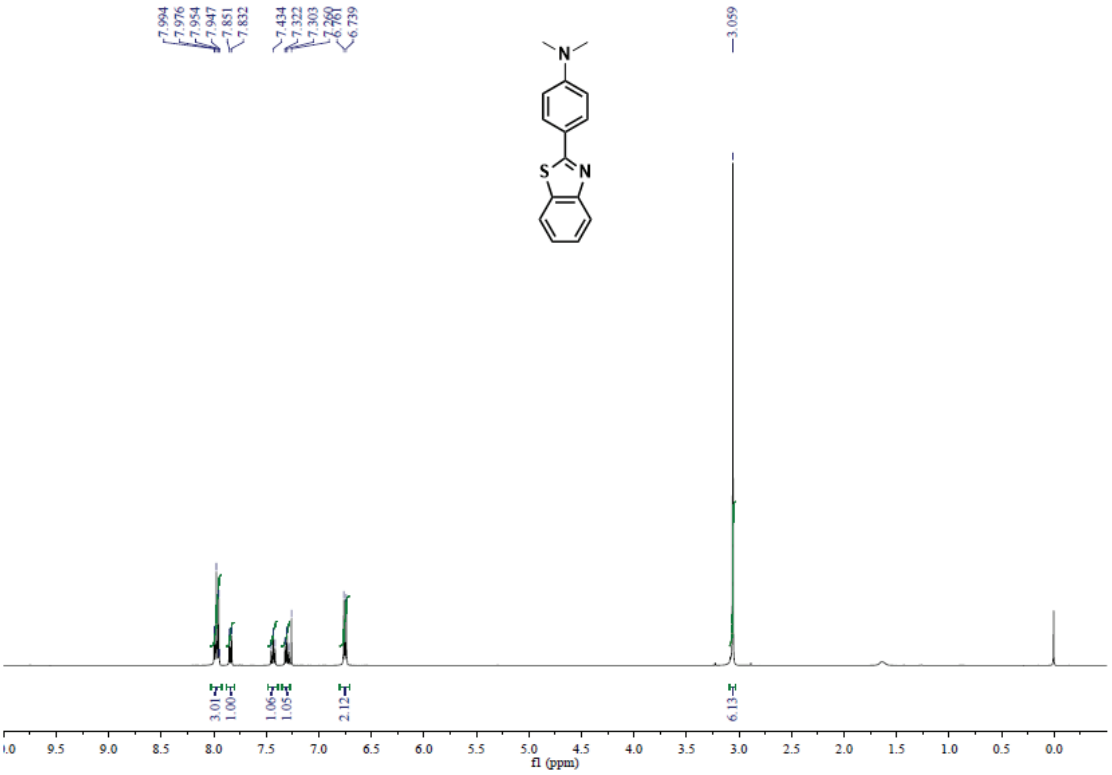

Fig. S1. ^{1}H NMR of **dmabt** (**1**) in $CDCl_3$.

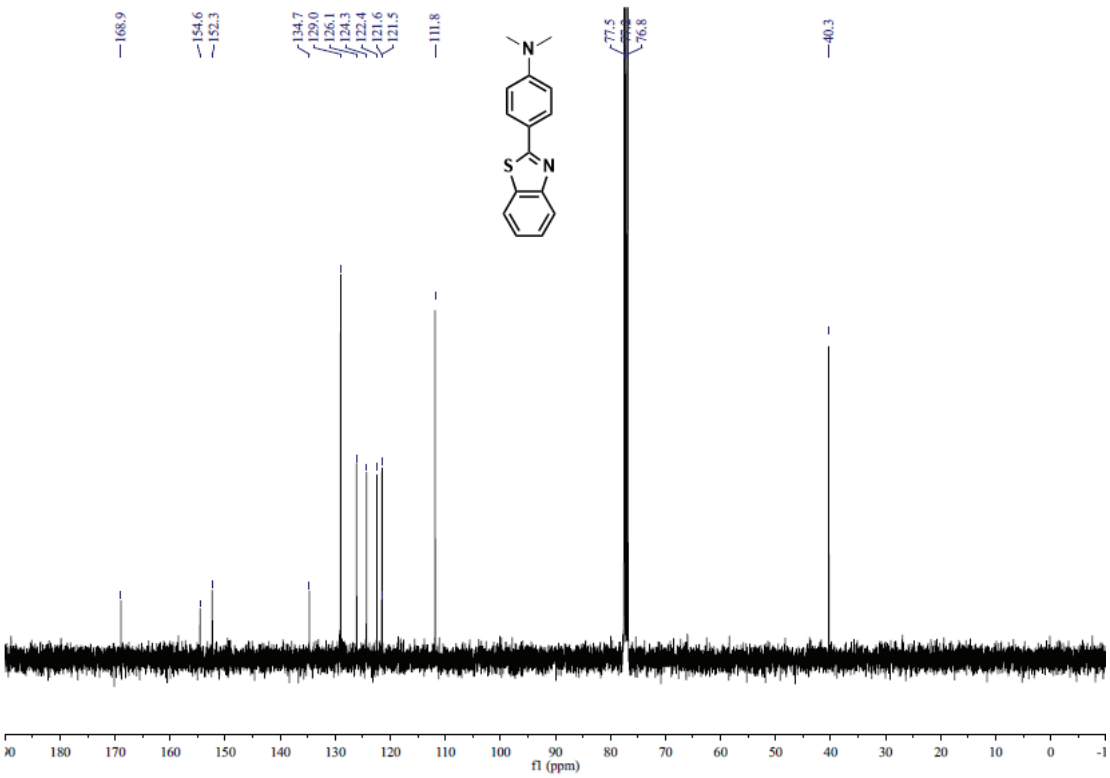

Fig. S2. ^{13}C NMR of **dmabt** (**1**) in $CDCl_3$.

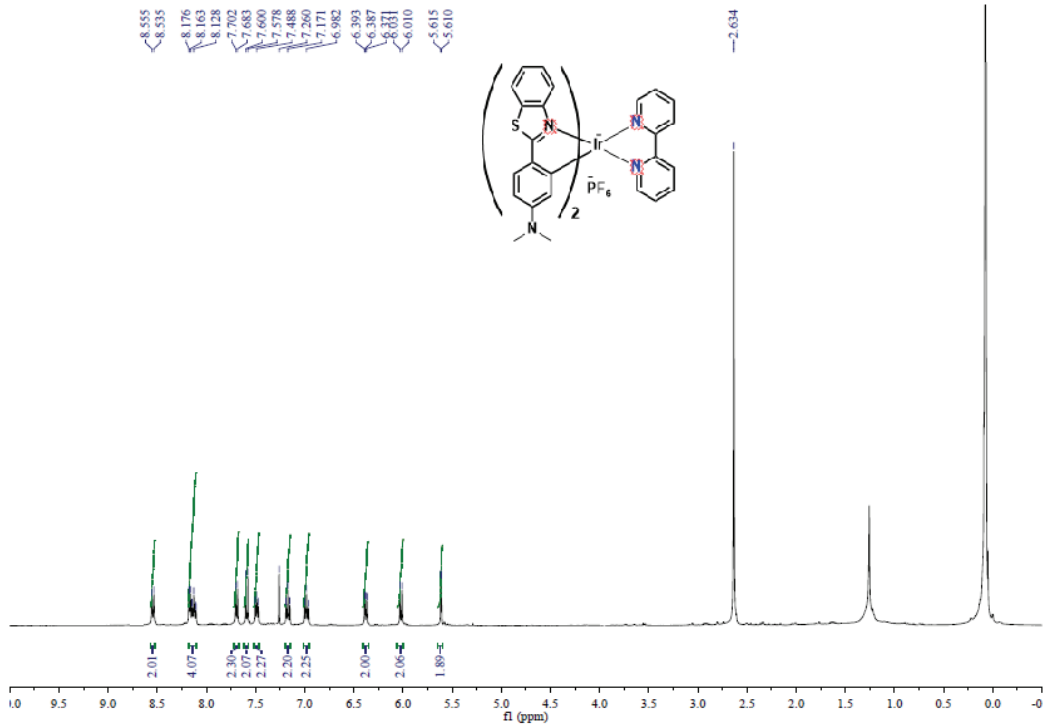

Fig. S3. ^{1}H NMR of **[Ir(dmabt)$_2$(bipy)][PF$_6$]** (**3**) in $CDCl_3$.

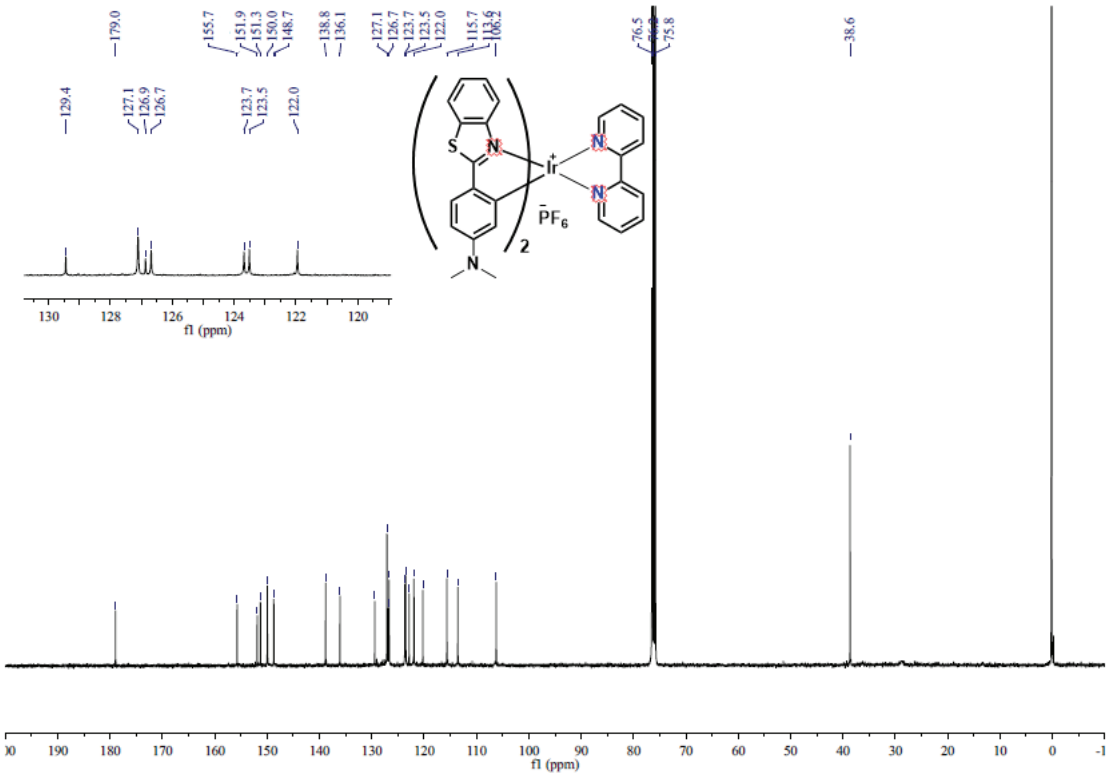

Fig. S4. ^{13}C NMR of **[Ir(dmabt)$_2$(bipy)][PF$_6$]** (**3**) in $CDCl_3$.